INSTITUTE OF PHYSICS PUBLISHING SMART MATERIALS AND STRUCTURES
Smart Mater. Struct. **16** (2007) S155–S169 doi:10.1088/0964-1726/16/1/S16

An experimental method to measure initiation events during unstable stress-induced martensitic transformation in a shape memory alloy wire

M A Iadicola[1,3] **and J A Shaw**[2]

[1] Metallurgy Division, Materials Science and Engineering Laboratory, National Institute of Standards and Technology, Gaithersburg, MD, USA
[2] Department of Aerospace Engineering, The University of Michigan, Ann Arbor, MI, USA

Received 12 April 2005, in final form 16 May 2006
Published 15 January 2007
Online at stacks.iop.org/SMS/16/S155

Abstract
An experimental configuration is demonstrated that captures features of the initiation of unstable stress-induced transformation in a shape memory alloy (SMA). The apparatus uses circulating fluids through the grips and a heat sink and thermoelectric devices to control the temperature profile of a specimen within a mechanical testing machine. The configuration can be used to restrict the initiation of phase transformation to a small region of interest of the free length, while permitting full-field optical tracking, infrared imaging, use of laser extensometry, and monitoring of load and extension. In this way, some longstanding difficulties in the measurement of thermo-mechanical phenomena in SMA wire have been resolved. The size of initiation stress peaks can be accurately measured for both transformation directions without changing the wire geometry, the temperature of a region of interest can be selected over a wide range, and imaging can be performed for multiple loading cycles and for events that occur from static to near dynamic rates. The motivation for this work is to produce high quality data for use in calibrating numerical models that study thermo-mechanical coupling during unstable transformation behavior.

1. Introduction

Shape memory alloys (SMAs) exhibit two prominent properties, the shape memory effect (where strains of the order of 8% can be recovered upon moderate heating, ≈10 to 20 °C) and pseudoelasticity (where similar strains are immediately recovered upon unloading). These behaviors are a result of a reversible martensitic transformation that may be induced by a change in temperature or stress. The high temperature low strain phase is called austenite (A), and has a $B2$ crystal structure with cubic symmetry. The low temperature or high strain phase is called martensite. It has a low degree of symmetry ($B19'$ structure in NiTi with monoclinic symmetry), resulting in a randomly oriented and twinned structure (at low temperature and low stress) or a reoriented, possibly detwinned, structure (stress-induced martensite, often denoted as M^+ for uniaxial tension). Occasionally there is an intermediate R (rhombohedral) phase, but it has a relatively minor role on the shape memory or pseudoelastic behavior within only the first 0.5% strain. At temperatures where austenite is the stress-free phase, the material exhibits pseudoelastic behavior during mechanical loading/unloading (figure 1 above 12 °C, see table 1). The stresses required for transformation (loading $A \rightarrow M^+$ and unloading $M^+ \rightarrow A$) increase dramatically with increasing temperature (≈7.3 MPa °C^{-1} for the plateau stresses, see inset in figure 1), this is the well known thermo-mechanical interaction that is often described by the Clausius–Clapeyron relation.

NiTi is of great interest for applications, due to its ability to sustain both relatively large stresses and deformations. Many novel uses have been suggested to exploit these unique behaviors (Otsuka and Wayman 1998, Nguyen *et al* 2001, Kudva *et al* 2001, Rey *et al* 2001, Schwartz 2002). These

[3] Author to whom any correspondence should be addressed.

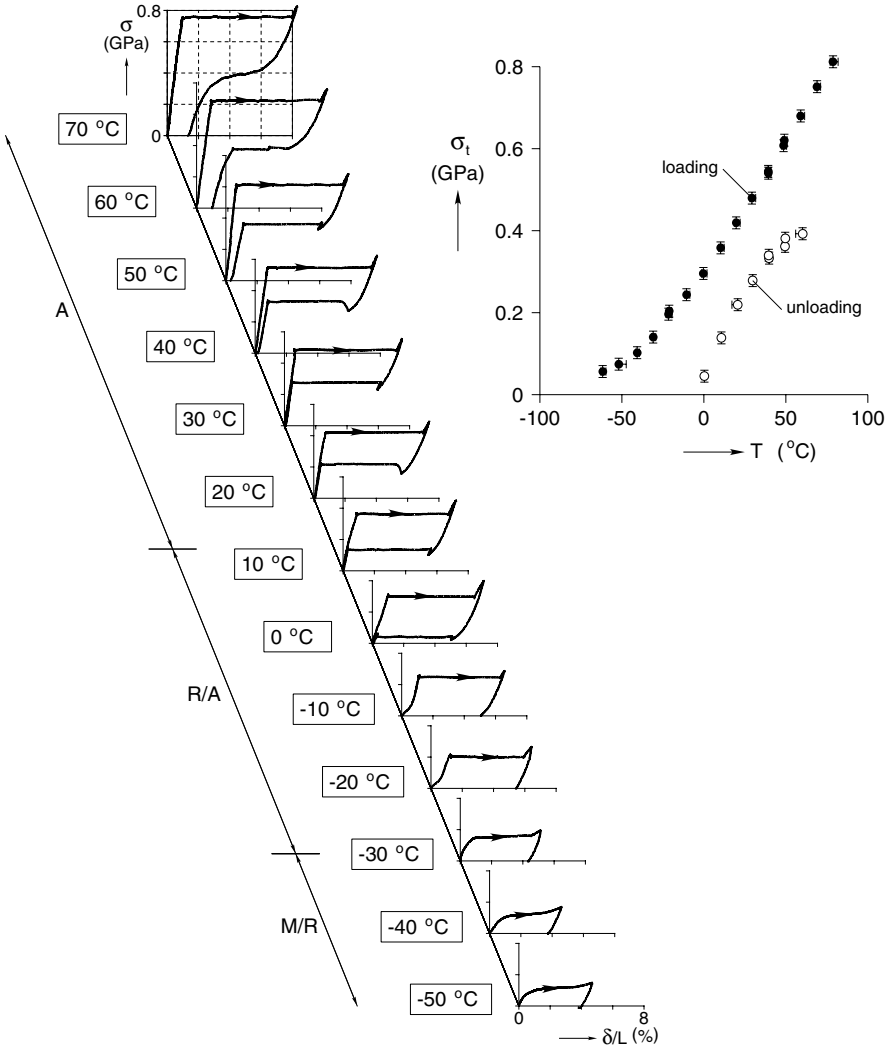

Figure 1. Isothermal uniaxial mechanical responses of virgin NiTi wire (performed in air chamber at $\dot{\delta}/L = 5 \times 10^{-5}$ s^{-1}). Propagation (plateau) stresses for transformation during loading ($A \rightarrow M^+$) and unloading ($M^+ \rightarrow A$) as a function of temperature (inset plot).

Table 1. Transition temperatures (±3 °C) and stress-free enthalpy (±3 J g^{-1}) for NiTi wire sample (95 mg) developed from differential scanning calorimetry (performed at 10 °C min^{-1}).

	A_s	A_f	R_s	R_f	M_s	M_f	$\Delta h_o^{M \rightarrow A}$
Values	−28	12	13	−29	−76	−118	15.3
Units	°C	°C	°C	°C	°C	°C	J g^{-1}

applications require a material that behaves reliably and predictably for a range of operating conditions. These requirements are often achieved through 'training', consisting of mechanical, thermal, or combined thermal mechanical cycling. These procedures are usually performed at high rates, which can result in a substantially reduced service life of the material. Currently, the most commonly used and least expensive form of NiTi is wire, thus our experiments are performed on NiTi wire specimens.

It is now well known that pseudoelastic polycrystalline NiTi exhibits unstable mechanical behavior during uniaxial stress induced transformation (Shaw and Kyriakides 1995, Liu *et al* 1998). This leads to distinctly non-uniform deformation fields as the specimen initiates substantial transformation ($A \rightarrow M^+$) in a localized length of the specimen accompanied by a sudden drop in load. During unloading, a sudden load rise is seen at the onset of localized $M^+ \rightarrow A$ transformation. It has been reported (Brinson *et al* 2004) that the material in the localized high strain region has a much higher fraction of tensile oriented martensite than the remainder of the length of the specimen, but still is not fully transformed to M^+ (only 60% to 70% for coarse grained, textured NiTi). Between this highly transformed (high axial strain, thinner diameter) region and the less transformed (lower axial strain, thicker diameter) region is a local region with a gradient in axial strain that we call a transformation front. For brevity in the remainder of this work, the high strain region is generally referred to as martensite (M^+) and the less transformed region is referred to as austenite, but we recognize that this is not strictly true at the micro-scale.

Local to any phase transformation is the generation (or absorption) of latent heat. This results in a local heating (or cooling) at the propagating transformation front and at

initiations of localizations. Thus, the specimen exhibits an evolving non-uniform temperature field. If the ambient environment cannot remove or supply this heat to keep the specimen isothermal, self-heating or cooling occurs. This interacts with the inherent temperature sensitivity of the transformation stresses (see inset in figure 1) resulting in a feedback loop that can manifest itself in the form of rate and environmental sensitivities (Shaw and Kyriakides 1995). These phenomena lead to the consideration of three principal timescales: (1) the imposed loading rate (quasistatic in our experiments); (2) the characteristic time for heat transfer (including conduction along the wire and convection to the ambient environment); and (3) the inherent time for martensitic transformation which is usually much smaller than (1) and (2) since it occurs at rates approaching the shear wave speed in the material.

Prior work shows that near isothermal conditions produce few localizations (and thus few fronts) and distinct plateaus in the mechanical response as seen in figure 1, whereas near adiabatic conditions produce numerous initiations of localizations (thus many fronts) and a more stable looking mechanical response. The number of initiation events has been shown to be related to the size of the initiation load drop ($A \rightarrow M^+$) or load rise ($M^+ \rightarrow A$) as compared to the non-uniform temperature field (Shaw and Kyriakides 1997), and this has been further investigated using quantitative finite element analyses (Shaw 2000, Iadicola and Shaw 2004). Results from a unique experimental arrangement to investigate low cycle behavior in SMAs (Iadicola and Shaw 2002a) suggest that sites of initiation are favorable locations for initiations during subsequent cycles. Additionally, the results show that the peak stress and size of the stress drop decrease with cycling, which was also reported in Gong *et al* (2002) and Shaw (1997) but was not investigated further.

Numerical modeling that incorporates the localized nature of the deformation as well as the latent heating/cooling without *a priori* definition of front kinetics is being developed (Shaw *et al* 2003). Modeling of SMA wire is done in one dimension and discontinuous strain fields are prevented by the use of a strain gradient approach, which is consistent with the observation that a transformation front is actually a propagating neck with a smooth radial profile. This model requires knowledge of the axial extent of a front for calibration purposes. Therefore, an investigation of the first initiation event (which is related to the front length and affects the size of the initiation stress peak) and repeated cycling of the initiation event are needed.

Complicating any investigation of the initiation of localized unstable behavior during loading is that any stress concentrations tend to mask the true size of the initiation. In other words, the problem is imperfection sensitive. Stress concentrations often occur in the gripping of the specimen and are typically avoided by tapering the specimen, which works for $A \rightarrow M^+$ only and cannot completely eliminate stress concentrations at the shoulder of the gage section. Furthermore, the thinning of a wire is difficult (although this was done in Tse and Sun (2000)) and machining risks affecting the mechanical properties of the material. These difficulties were substantially solved by controlling the ambient axial temperature distribution along the wire (see Iadicola and Shaw 2002b, 2002a). A similar experimental method is used here to focus on the behavior and characteristics of initiation events and how they are influenced by changes in temperature and repeated initiation.

2. Experimental objectives

We want to keep transformation activity in the gage (center exposed) section of the wire specimen (away from the grips) where the stress and temperature field are nearly uniform. In addition, we want to track the full-field temperature and deformation behavior of the initiation while simultaneously monitoring the load history for quasistatic elongation histories. Similar goals were accomplished in Iadicola and Shaw (2002b), where the region of interest (ROI) was most of the wire length. In this paper, we focus on a smaller ROI and assure that initiation events occur there (the experimental details will be discussed below). Additionally, we want data over a range of temperatures to investigate trends resulting from the strong thermo-mechanical coupling in the material. Two types of experiments will be presented: (1) high speed monitoring of a dynamic initiation event to capture the development and extent of initial $A \rightarrow M^+$ localization on loading (experimental set 1), and (2) low speed monitoring of the evolution of repeated initiation to capture the change in the initiation stress peak and the apparent change in the latent heat during cycling for $A \rightarrow M^+$ (experimental set 2) and $M^+ \rightarrow A$ (experimental set 3) transformations.

3. Experimental setup

The experimental arrangement originally described in Iadicola and Shaw (2002b) is modified to achieve the objectives described above (see figure 2). The SMA wire specimen is deformed in a uniaxial testing machine. All the experiments are performed on virgin samples taken from the same batch of NiTi wire (0.765 ± 0.002 mm diameter, table 1). The wire specimen is in contact with a custom-built thermal control apparatus that is connected to laboratory cooling water and a temperature-controlled fluid (silicone oil) circulating bath. A digital data acquisition system is used to simultaneously record multiple signals during displacement controlled tension tests. These signals include the crosshead displacement (control signal), load (5 kN load cell), elongation in the gage section (non-contacting, collimated sheet, laser extensometer), and the control and feedback signals of the thermal control apparatus.

A diagram of the thermal control apparatus is shown in figure 3. The wire specimen is clamped at each end by grooved steel grip plates which are in thermal contact with a copper heating pipe that has silicone oil circulating through it from the temperature controlled fluid bath (temperature range -40 to $150\,^{\circ}\mathrm{C}$). The center gage section of the wire is in thermal contact on the back side with an aluminum heat sink that is connected to laboratory cooling water (typically 15 to $20\,^{\circ}\mathrm{C}$). Although the copper heating pipe passes through the aluminum block, an insulation sleeve is located between the heating pipe and the aluminum heat sink. These two fluid systems allow the temperature of the wire specimen at the grips and along the gage length to be controlled independently while retaining proper alignment between the

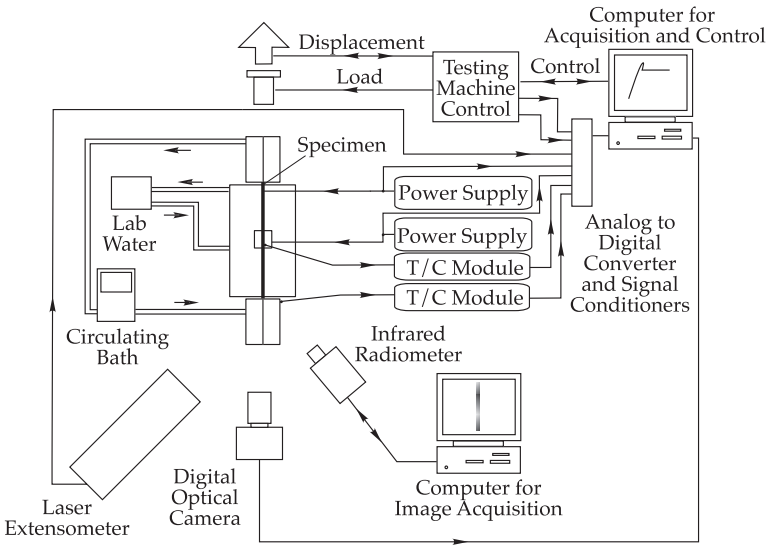

Figure 2. Experimental arrangement.

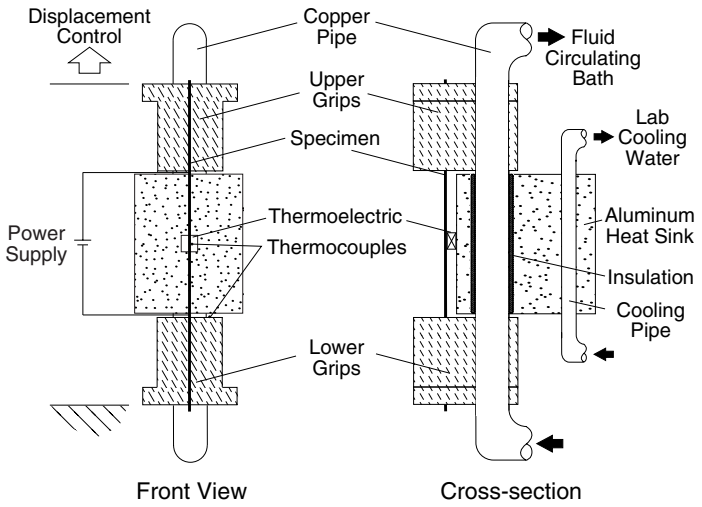

Figure 3. Thermal control apparatus.

grips and block. A thermoelectric module (along with an aluminum shim to precisely fill the horizontal gap) is placed between the back side of the specimen and the aluminum heat sink. Various configurations of the thermoelectric modules may be used along the gage length to locally cool/heat the gage section of the wire to create an ambient temperature field. Note: this method has been shown to maintain the ambient temperature field of a wire very effectively, even with self heating/cooling, (Iadicola and Shaw 2002b), except during the dynamic initiation events and at strain rates $\geqslant 10^{-3}$ s^{-1} (Iadicola and Shaw 2002a). Two thermoelectric modules are used in this work 6 mm × 6 mm (Melcor CP0.8-7-06L) and/or 12 mm × 12 mm (Melcor CP0.8-31-06L[4]). A thermally conductive, electrically insulating silicone paste (Omegatherm 201, thermal conductivity $k = 2.3$ W K^{-1} m^{-1}) is used to ensure good thermal contact between the wire and the thermoelectric modules. The front face of the wire is exposed and available for full-field optical and infrared imaging and laser extensometry. The gradient in temperature across the diameter of the wire is considered negligible if the Biot number (the non-dimensional ratio of the lateral thermal resistance to the boundary thermal resistance) is much less than unity. In our case, this number has been estimated to be of the order of 10^{-4} (see Iadicola and Shaw 2002b). Fine wire thermocouples (0.079 mm diameter wire, exposed junction, K type) are set into the silicone paste to monitor the local temperature. The thermocouple signals are amplified using thermocouple modules, and this arrangement is calibrated by ASTM certified glass thermometers at two temperatures that span the limits of the experiment. The total gage section of the wire is connected to a DC power supply (maximum output 8 V at 20 A) to allow for joule heating of the wire.

[4] Certain commercial equipment, instruments, or materials are identified in this paper in order to specify the experimental procedure adequately. Such identification is not intended to imply recommendation or endorsement by the National Institute of Standards and Technology, nor is it intended to imply that the materials or equipment identified are necessarily the best available for the purpose.

As mentioned above, the $A \rightarrow M^+$ transformation initiation peaks are often not observed or are of reduced size due to stress concentrations at the grips. The ability to control the temperature along the wire in conjunction with the fact that the transformation stress is a strongly increasing function of temperature (typically 7 to 9 MPa $^\circ C^{-1}$ for $A \rightarrow M^+$) allows us to overcome this problem. Heating the grips (using the fluid bath) and free length (by joule heating) of the wire raises the stress required for $A \rightarrow M^+$ transformation. Cooling the portion of the wire in contact with the thermoelectric module lowers the stress of transformation in that local area. Transformation can be initiated away from the grips without the need to thin a portion of the specimen. In other words, the imposed temperature field is used to develop graded properties along the wire length for the purpose of studying instability features in the material behavior. The approximate location of initiation can be chosen through selection and positioning of the thermoelectric modules (either the 6 mm or 12 mm modules).

A digital infrared imaging system (Inframetrics ThermaCam SC1000 with a PtSi 256 × 256 detector array) monitors the evolution of temperature along a selected portion of the specimen length from the front of the specimen. The maximum digital acquisition rate for this system is 60 frames per second (fps), where each frame is an average of the infrared energy over about 1/60 s. The accuracy of the temperature measurement from the infrared imaging system depends on knowledge of the emissivity of the specimen. This is calibrated by coating a portion of the surface of a wire sample with paint of known emissivity near unity and heating the sample above the ambient temperature. The sample is imaged and the temperature is measured in the area of known emissivity. Then the emissivity is adjusted down until the temperature in the uncoated portion of the wire matches that measured earlier. This is the calibration procedure recommended by the manufacturer and gives an emissivity of about 0.66 (±0.05) in our case. It should be noted that the emissivity of the wire might change somewhat when transformed from austenite to martensite. In Shaw and Kyriakides (1997), for example, the emissivity of the strip material changed from 0.83 to about 0.86 during the initial transformation from austenite to martensite. However, the emissivity change was more dependent on the surface condition of the specimen than on the particular material phase. The NiTi strip material used in that study was heavily oxidized with a black coating that resulted in a noticeable change in the surface roughness and an optical color change to a light gray color after the transformation. The surface oxide acted like a brittle coating that was disturbed by the transformation strain. In the present case, in contrast, the wire has only a fine oxide layer, light bronze color, with no noticeable change in color during the transformation. Therefore, we consider a 0.05 variability in the emissivity to be a very conservative upper bound, and it is doubtful that an emissivity change led to a significant temperature uncertainty.

Optical imaging is performed using a digital camera to monitor the reflection of an appropriate light source off of the specimen. The transformation front is the leading edge of a small propagating neck that can be seen by the naked eye under proper lighting conditions. Digital filtering of the intensity distribution of the reflected light allows transformation fronts to be located (Iadicola and Shaw 2002b). One of two cameras is used: either a low speed, high resolution, digital camera system (1300 × 1030, 12 bit detector array, with 5 MHz controller, maximum of 3 fps); or a high speed, lower resolution, digital camera system (Kodak HRC1000 512 × 384, 8 bit detector with 1000 fps acquisition). Although a common fluorescent light is used for the low speed imaging, high speed imaging requires a high intensity halogen bulb lighting (1000 W) with multiple infrared filters between the light and the specimen to minimize unwanted effects on the infrared imaging system.

There are many uncertainties associated with the various quantities measured here, and they result in quantifiable uncertainties in the reported data (all uncertainties in this paper are based upon one standard deviation). The reported engineering stress ($\sigma = P/A_o$) has an uncertainty of ±1.4 MPa, whereas the measured plateau stress level (σ_t) is ±15 MPa due to variations in the stress along the plateau. The size of the initiation stress peak ($\Delta\sigma$) has an uncertainty of ±7 MPa, due partially to the judgment of the plateau level. The axial strain (ε) is measured based upon either grip displacement/free length (δ/L) with an uncertainty of ±0.015% or based upon laser extensometer tag relative displacement/initial tag separation (ε_{LE}) with an uncertainty of ±0.008%, but is subject to occasional tag shifting that results in sudden ±0.26% changes in strain (especially at changes in loading direction). For both infrared and optical imaging techniques, the judgment of position is dependent upon the resolution of the image. The measurements used below for axial location are positions along the thermoelectric module of interest normalized by either the length of the thermoelectric module (x/L_{TE}) or initial wire diameter (x/d_o). The uncertainties for x/L_{TE} and x/d_o for the infrared results are ±0.02 and 0.15, respectively; whereas the uncertainties for the high speed optical imaging are ±0.004 and 0.018, respectively. The time resolution of the analog data signals is ±15 ms, but is reduced to ±8 and 0.5 ms for the infrared and high speed optical imaging, respectively. The uncertainty in the temperature needs to be described in terms of the absolute and relative uncertainties. Unfortunately, absolute temperature measurement is difficult and results in an uncertainty of about ±5 °C. Our relative temperature measurement for ambient experimental temperature is about ±1.5 °C (but increases to ±4 °C for experiments using the high intensity lighting). The relative temperature measurement within each experiment is about ±0.2 °C for the infrared imaging (ΔT), peak change in temperature profiles (ΔT_{peak}), and maximum temperature peaks (ΔT_{max}).

4. Experimental results

Three sets of experiments are described below to demonstrate the experimental method. Each set requires a slightly different configuration of thermoelectric modules and temperature control (see figure 4). Experiment set 1 is an investigation of the transient mechanical and thermal behavior within the first two seconds of $A \rightarrow M^+$ initiation. Experiment set 2 is concerned with the measurement of the initiation stress peak and latent heating during $A \rightarrow M^+$ transformation for multiple cycles and various temperatures. Experiment set 3 is similar to

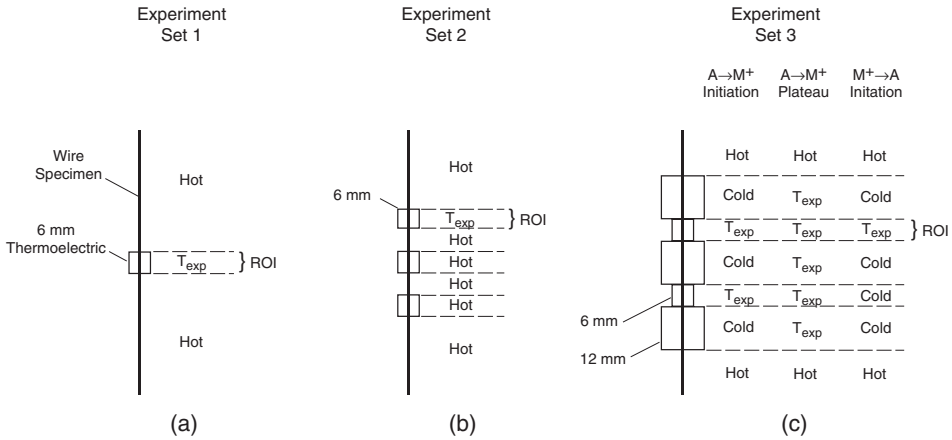

Figure 4. Thermoelectric module configurations and temperature control for (a) experiment set 1, (b) experiment set 2, and (c) experiment set 3. The labels hot and cold are in comparison to the experimental temperature setting (T_{exp}).

experiment set 2, but addresses the $M^+ \rightarrow A$ transformation during unloading. All three sets of experiments are performed in displacement control at a nearly static nominal strain rate of $\dot{\delta}/L = 10^{-4}\ \mathrm{s}^{-1}$.

4.1. Experiment set 1

Experiment set 1 uses a single 6 mm × 6 mm thermoelectric module near the center of the gage section, heated grips, and joule heating along the free length (see figure 4(a)). Throughout the experiment, the grips and portion of the specimen between the grips and center thermoelectric module are kept at elevated temperatures while the center of the specimen in contact with the thermoelectric module is held at a lower temperature (T_{exp}). For example, in one of the experiments below performed at $T_{exp} = 22\,^{\circ}\mathrm{C}$, the grips temperature is near 54 °C and the temperature of the specimen between the grips and the thermoelectric module is approximately 40 °C. During loading, the initiation of localization occurs in the portion of the specimen that requires the lowest $A \rightarrow M^+$ transformation stress as shown in figure 5(a) (i.e., the cooler region in contact with the thermoelectric module, figure 4(a)). Laser extensometer retro-reflective tags (not shown) are attached to the wire just above and below the thermoelectric module giving a 12 mm nominal initial spacing. Optical images are taken using the high speed camera and a 60 mm macro lens at 1000 fps, resulting in an image resolution of approximately 47 pixels mm^{-1}. The infrared images are taken at the maximum system speed of 60 fps (with an approximately 9 pixels mm^{-1} resolution) where a trigger signal is used to synchronize the digital images and the other data signals. The region across the thermoelectric module is monitored by the infrared and high speed optical cameras which are buffered and triggered after the initiation event, thus capturing the behavior in the temporal vicinity of the event. After the initiation, the loading is stopped and the specimen is unloaded.

Two experiments are performed in this set, one at a thermoelectric module temperature of 22 °C (experiment 1A shown in figure 6), and one at 34 °C (experiment 1B shown in figure 7). Figure 6(a) shows the engineering stress versus axial strain response of the wire (where P is the load and A_o is the initial wire cross-sectional area) for $A \rightarrow M^+$ initiation at 22 °C. The apparent 'strain', ε, is measured two ways, grip displacement/wire free length (solid line) and relative laser extensometer tag displacement/initial tag distance (dashed line). Initiation occurs at point 'a' and is nearly complete by point 'b'. The height of the initiation stress peak ($\Delta\sigma^{A\rightarrow M^+} = (P_{peak} - P_{plateau})/A_o$) is 74 MPa which (similar to Tse and Sun 2000, Iadicola and Shaw 2002b, 2002a) is substantially larger than that observed in the past (Shaw and Kyriakides 1997, Shaw 1997, Gong *et al* 2002), thus we seem to have substantially minimized the effect of 'imperfections' that would otherwise mask or reduce the peak.

The change in temperature (ΔT) is calculated by subtracting a reference infrared image from each current infrared profile. Each profile is extracted from a 4 pixel wide (≈85 μm or ≈11% of the specimen diameter) thin strip in the infrared image. Each profile is converted to a thin color contour plot, and 81 such profiles are shown side-by-side along the timescale in figure 6(b), where x is the position along the length of the thermoelectric module ($L_{TE} = 6$ mm). Figure 6(d) shows an optical intensity plot developed from the changes in reflected light compared to (subtracting) a reference state before initiation in the thermoelectric module region of the specimen (from a time just before point 'a'). Both the reference and the current images are smoothed (low-pass filtered) before subtraction. A particular axial profile is taken at a fixed location along the width of the specimen that best shows the reflection change during the initiation event resulting in figure 6(d). The transformed region (M^+) is shown by the expanding white region of the plot. The axial location and time of the initiation event can be seen in both figures 6(b) and (d).

Figure 6(c) plots the load and laser extensometer strain for the same time period as for figures 6(b) and (d). During the 2 s shown, the grip displacement changes by less than 0.014 mm, so the displacement boundary conditions can be considered fixed during the initiation event (see also the near vertical drop in load in figure 6(a) between times 'a' and 'b' for the solid curve based on grip displacement). The streak plot in figure 6(d) shows that the extent of the localization is initially 0.6 wire diameters (occurring within 1 ms) and develops to

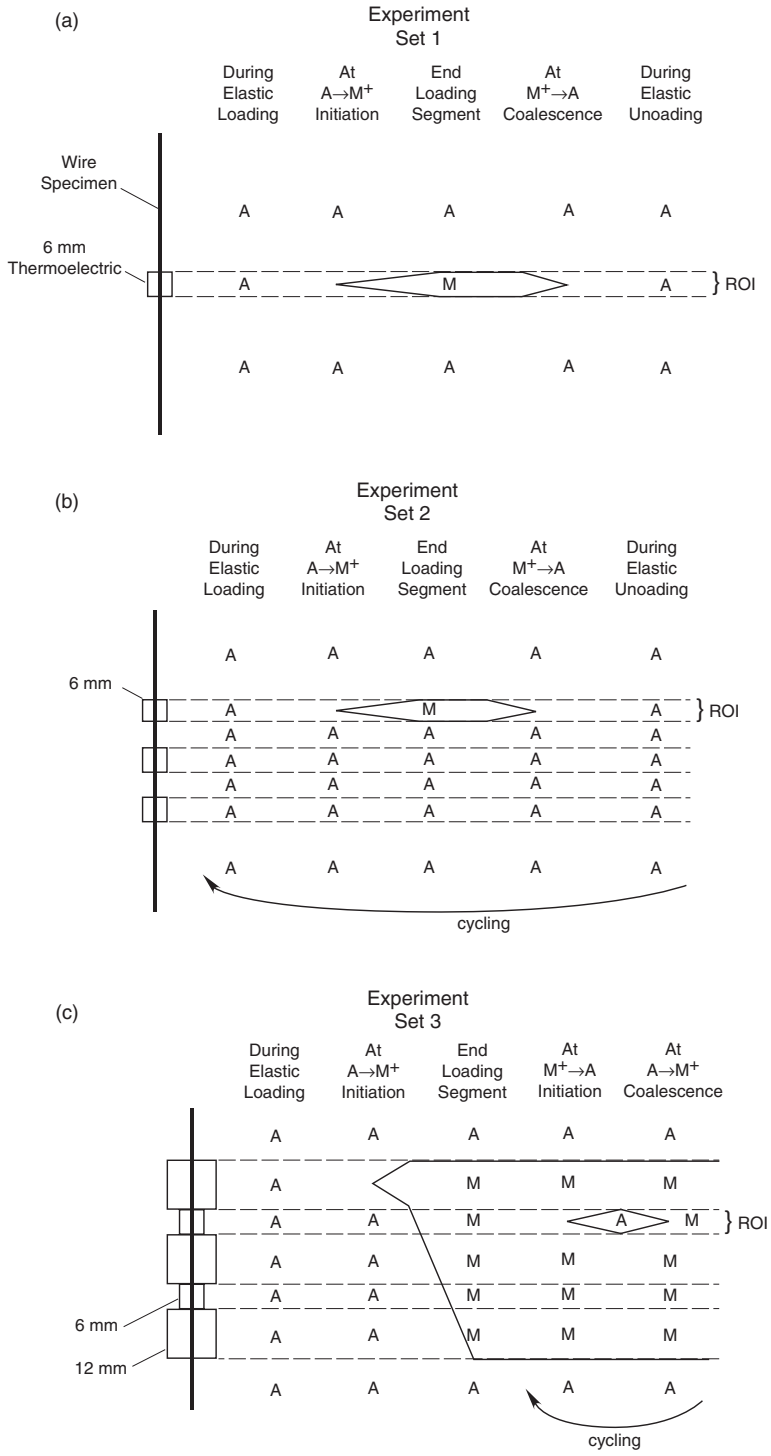

Figure 5. Schematic of austenite (A) and martensite (M) phases (transformation fronts shown by solid lines) during various stages corresponding to figure 4 for (a) experiment set 1, (b) experiment set 2, and (c) experiment set 3.

1.4 wire diameters over 0.27 s. Then the transformed region grows to 2.7 diameters during the next 0.89 s, and remains nearly constant for the remaining time shown. One can notice correspondence between these changes in the extent of the neck (figure 6(d)) and changes in the slope of the laser extensometer strain figure 6(c). Note the changes in slope at times 174.39 s (initiation), 174.66 s (end of initial development), 175.55 s (full development), and 175.69 s (slight variation). The temperature plot in figure 6(b) shows that the extent of the initial temperature bloom is 1.6 wire diameters and lasts for only 0.03 s and is followed by a decay over 0.5 s to near the background temperature. The peak temperature change seen is 11.6 °C, which is less than the adiabatic temperature rise of 30.6 °C estimated from the stress-free enthalpy and specific

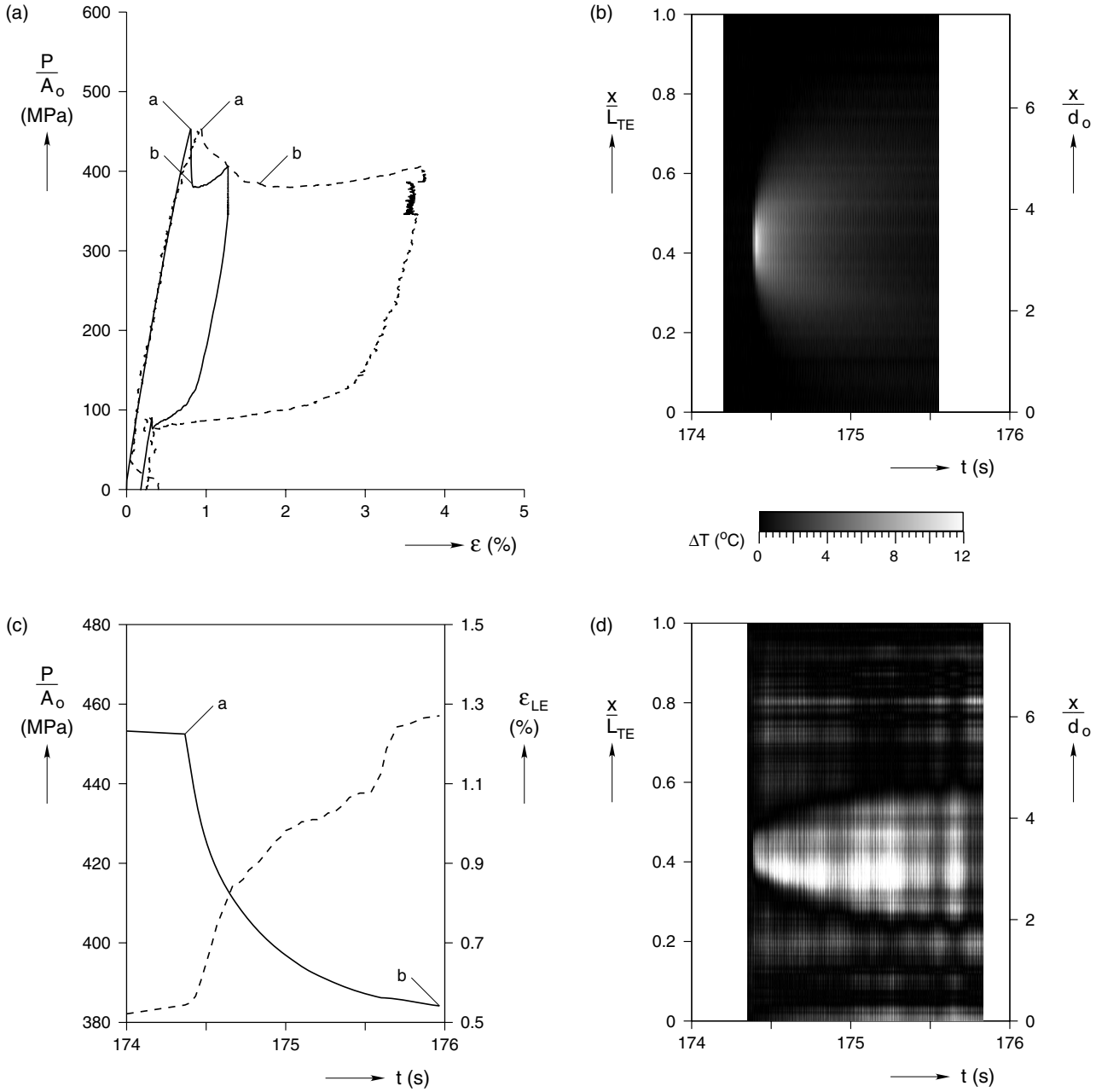

Figure 6. Results of experiment 1A performed at 22 °C: (a) engineering stress versus axial strain calculated from grip displacement/free length (solid line) and laser extensometer tag relative displacement/initial tag separation (dashed line); (b) temperature change derived from infrared images of wire within 6 mm thermoelectric region taken at 60 Hz; (c) engineering stress (solid line) and laser extensometer strain (dashed line) versus time; and (d) intensity plot developed from optical images taken at 1000 Hz.

heat,

$$\frac{\Delta h}{C_o} = \frac{15.3\ \mathrm{J\ g^{-1}}}{0.5\ \mathrm{J\ g^{-1}\ K^{-1}}} \approx 30.6\,^{\circ}\mathrm{C}.$$

This shows that the active cooling from the thermoelectric module is effective in keeping the specimen isothermal, except for a short moment at the onset.

A second experiment, experiment 1B, is performed at a higher temperature ($T_{\mathrm{exp}} = 34\,^{\circ}\mathrm{C}$ with a different portion of the same wire specimen that has never been transformed) and the results are shown in figure 7. Again the boundary conditions can be considered fixed during the initiation event since the grip displacement changes by less than 0.014 mm during the 2 s shown in figures 7(b)–(d). The streak plot in figure 7(d) shows that the extent of the localization is initially 0.8 wire diameters (occurring within 1 ms near $x/L_{\mathrm{TE}} = 0.6$) and develops to 1.8 wire diameters over 0.25 s. (The white streak near $x/L_{\mathrm{TE}} = 0.2$ is an artifact of the image processing and should be ignored.) The transformed region then grows to 2.8 diameters during the next 0.78 s, and continues to grow through the remainder of the time shown. Comparing these results to experiment 1A shows that the length of the initiation

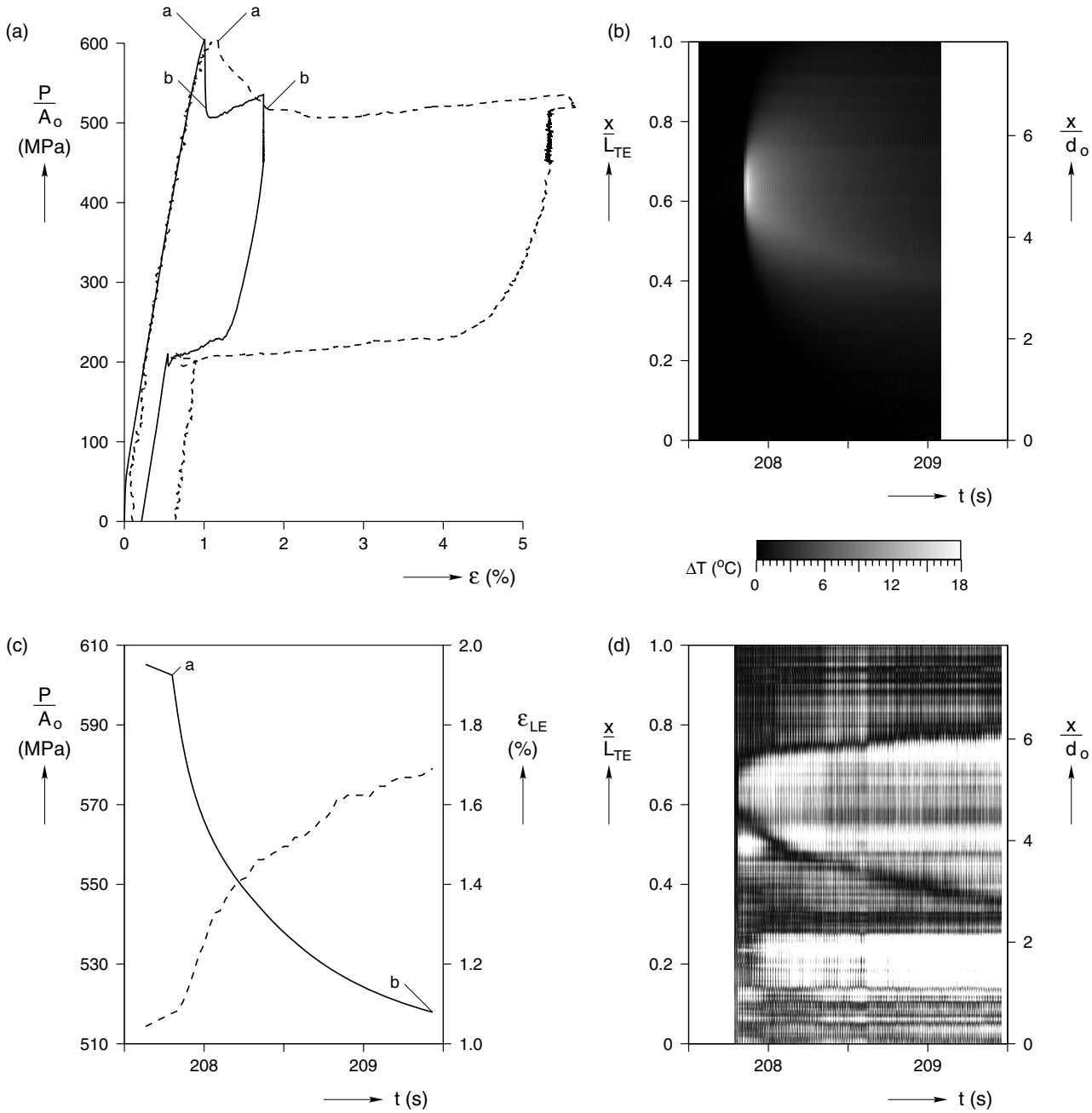

Figure 7. Results of experiment 1B performed at 34 °C: (a) engineering stress versus axial strain calculated from grip displacement/free length (solid line) and laser extensometer tag relative displacement/initial tag separation (dashed line); (b) temperature change derived from infrared images of wire within 6 mm thermoelectric region taken at 60 Hz; (c) engineering stress (solid line) and laser extensometer strain (dashed line) versus time; and (d) intensity plot developed from optical images taken at 1000 Hz.

region increases with stress level. Again there appears to be correlation between these changes in the extent of the neck (figure 7(d)) and changes in the slope of the laser extensometer strain figure 7(c). Note the changes in slope at times 207.80 s (initiation), 208.05 s (end of initial development), and 208.83 s (middle of continuing growth and slope changes continuously). The temperature plot in figure 7(b) shows that the extent of the initial temperature bloom is 1.7 wire diameters and lasts for only 0.05 s and decays quickly (0.5 s) to near the background temperature. The peak temperature change seen is 17.5 °C, which is greater than in experiment 1A but still less than the adiabatic temperature rise.

4.2. Experiment set 2

Experiment set 2 uses three 6 mm × 6 mm thermoelectric modules spaced evenly along the length of the aluminum heat sink (see figure 4(b)). The three thermoelectric modules are independently controlled, which allows the user to choose one as the region of interest while the others are not being used

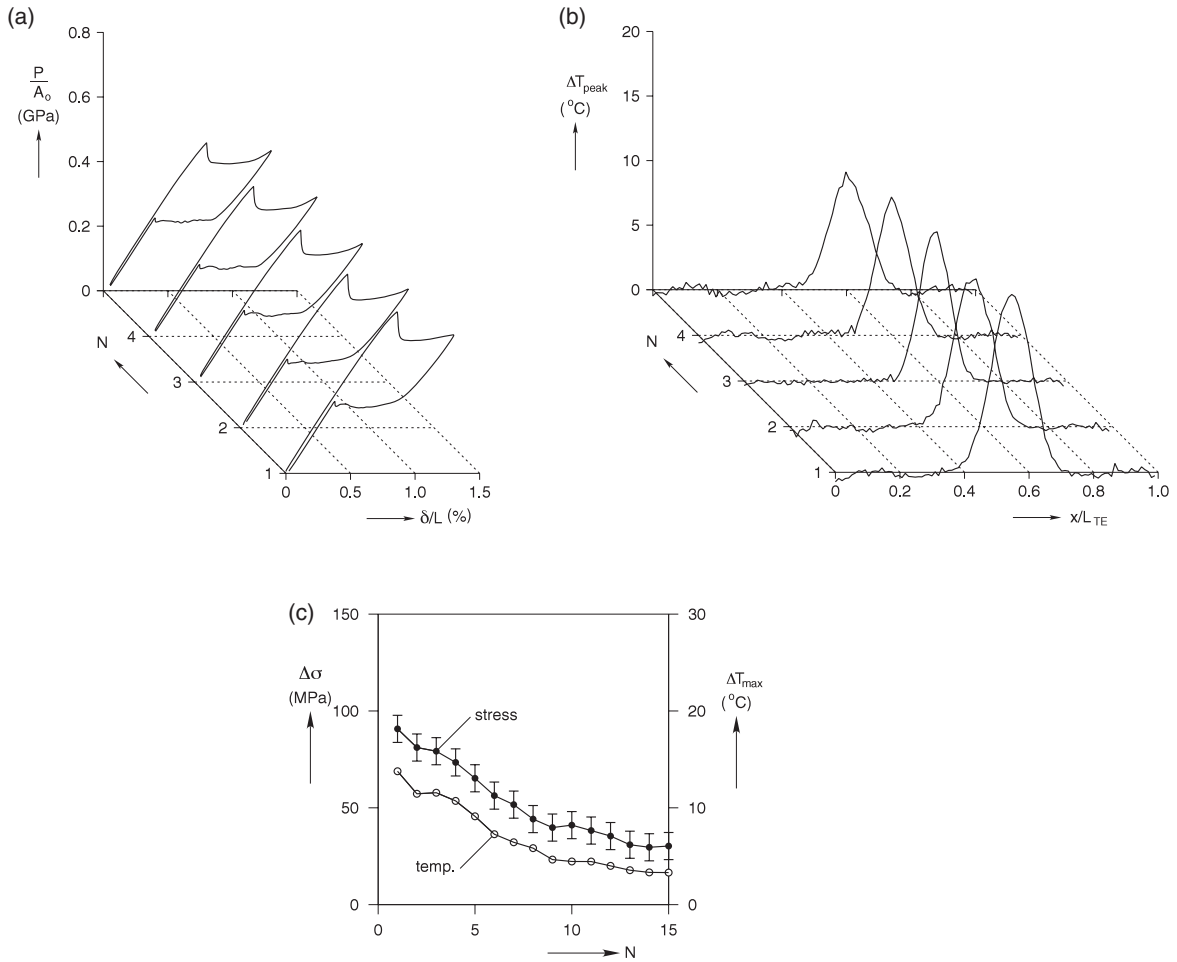

Figure 8. Results of experiment 2A performed at 23 °C: (a) load–displacement for the first five cycles; (b) change of temperature profiles for the first five cycles; and (c) change in maximum stress and maximum temperature rise versus cycle number (uncertainties associated with the $\Delta T_{\max}$ data points are less than the size of the data points shown).

(see ROI in figure 4(b)). This allows one specimen to be used in three separate experiments as if using a virgin specimen in each case. A series of cyclic initiation experiments are conducted at two different temperatures, as shown in figure 8 (23 °C, experiment 2A) and figure 9 (40 °C, experiment 2B). The high resolution optical camera is used rather than the high speed camera, and infrared imaging is performed similar to experiment set 1. Both are focused on the current 6 mm ROI. The grips are heated and joule heating is applied to the free length to maintain the wire at an elevated temperature except in the ROI. One thermoelectric module (the ROI) is held at a reduced temperature, but the other two thermoelectric modules are raised in temperature to avoid transformation occurring there. (Note this is especially needed for areas used previously for this type of experiment where a reduced initiation stress exists due to transformation cyclic softening.) After initiation, loading is continued until the stress rises somewhat, indicating that the ROI is fully transformed and the fronts (solid lines in figure 5(b)) begin to propagate in hotter regions outside of the ROI (figure 5(b), end loading segment). During unloading, the existing fronts propagate towards one another and then coalesce (figure 5(b), $M^+ \rightarrow A$ coalescence). The specimen then elastically unloads and displacement is stopped just prior to zero load. This constitutes the first cycle. The specimen is then cycled (loaded and unloaded) again while being subjected to the same temperature field (figure 4(b)), resulting in re-initiation in the same ROI. The mechanical cycling is then repeated several times until a stress peak is no longer discernible.

Figure 8(a) shows a plot of the load-displacement response of a specimen for a 15 cycle experiment performed at a nominal thermoelectric module temperature of 23 °C (experiment 2A). Only the first five cycles (N) are shown here for brevity. Profiles of the axial temperature distribution at the time of the maximum temperature peak (ΔT_{peak}) in each cycle is plotted in figure 8(b). This temperature peak is a transient event as seen in experiment set 1, so figure 8(c) shows the maximum change in temperature ($\Delta T_{\max}$) that occurs in each profile and $\Delta\sigma^{A\rightarrow M^+}$ for each cycle for all 15 cycles. The location of the $\Delta T_{\max}$ peak along the length of the profile shifts slightly ($x/L_{\text{TE}} \approx \pm 0.05$) with increasing cycling, as the axial extent of the maximum temperature profiles stays relatively constant ($x/L_{\text{TE}} = 0.40$ to 0.75). The tendency of $A \rightarrow M^+$ initiation at sites of previous $A \rightarrow M^+$ initiation is consistent with behavior shown in Iadicola and Shaw (2002a). As the stress peak is reduced by cycling, the maximum temperature is also reduced, which is

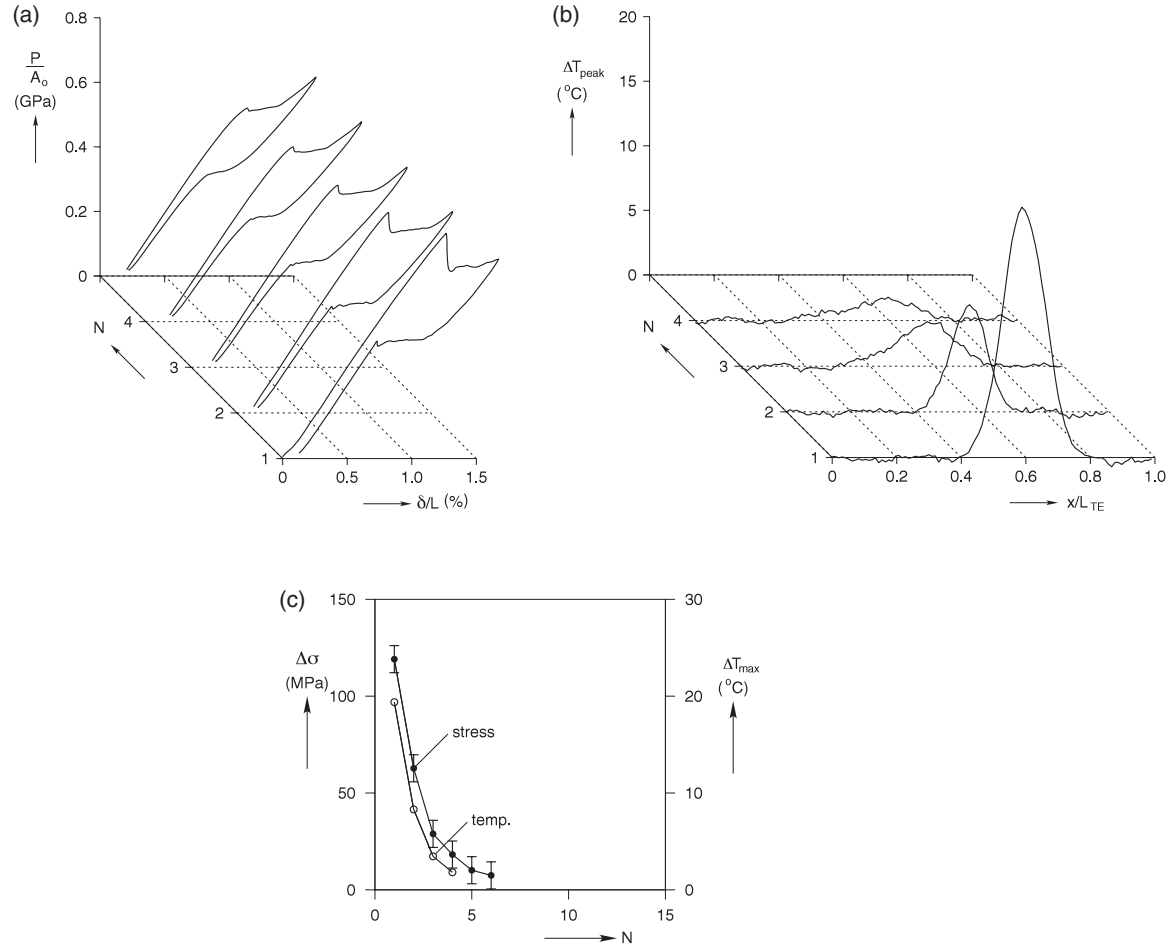

Figure 9. Results of experiment 2B performed at 40 °C: (a) load–displacement for the first four cycles, no discernible change in cycle 5; (b) change of temperature profiles for the first five cycles; and (d) change in maximum stress and maximum temperature rise versus cycle number (uncertainties associated with the $\Delta T_{\max}$ data points are less than the size of the data points shown).

expected as residual martensite and plasticity effects grow. We leave further discussion of these interesting effects to future work.

Figure 9 shows the results for experiment 2B performed at a nominal temperature of 40 °C with the ROI switched to another small thermoelectric module. The mechanical response with cycling is plotted in figure 9(a). The initiation peak is still present for the first five cycles, but the evolution is more dramatic than that shown in figure 8(a). The change in axial temperature profiles for these cycles (figure 9(b)) shows a larger temperature spike in the first cycle but then a rapid decrease in this peak with subsequent cycles. By cycle 5 no discernible temperature peak is seen in the profile. Only minor shifting of the peak location along the length is seen, but the axial extents of the peaks do vary slightly. In the first, third, and fourth cycles the peak is located roughly between $x/L_{\mathrm{TE}} = 0.4$ and 0.8; whereas, the extent of the peak is reduced in cycle 2 to about $x/L_{\mathrm{TE}} = 0.4$ and 0.7. Again the results for the experiment are summarized in figure 9(c) where a strong correlation is observed. Similar to the results for experiment 2A, these behaviors are due in part to residual martensite and plasticity effects. As seen in figure 1, residual strains for even the first cycle begin to develop between 30 and 40 °C. Thus, the plasticity effect should be more prevalent in experiment 2B (performed at 40 °C) than in experiment 2A (performed at 23 °C).

4.3. Experiment set 3

Since $A \rightarrow M^+$ nucleations have sometimes been observed to be preferred sites for $M^+ \rightarrow A$ initiation, the measurement of the evolution of $M^+ \rightarrow A$ initiation with cycles is also needed. While this is somewhat more difficult to measure due to the interaction of previous $A \rightarrow M^+$ cycles, it has been achieved with a multiple thermoelectric module setup that allows repeated initiation of A in a region of M^+ that has seen only one $A \rightarrow M^+$ front traversal and no initiation events. Experiment set 3 uses three 12 mm × 12 mm thermoelectric modules, each separated by a 6 mm × 6 mm thermoelectric module (see figure 4(c)). Again, the grips are heated and joule heating is applied to the free length. The imaging systems remain the same as in experiment set 2. Unlike the previous experiments, we now require the initiation on loading ($A \rightarrow M^+$) to occur outside the ROI, since this may affect later unloading initiations ($M^+ \rightarrow A$).

Similar to the previous experiments, one 6 mm thermoelectric module is selected as the ROI. During loading, the three 12 mm thermoelectric modules are cooled below

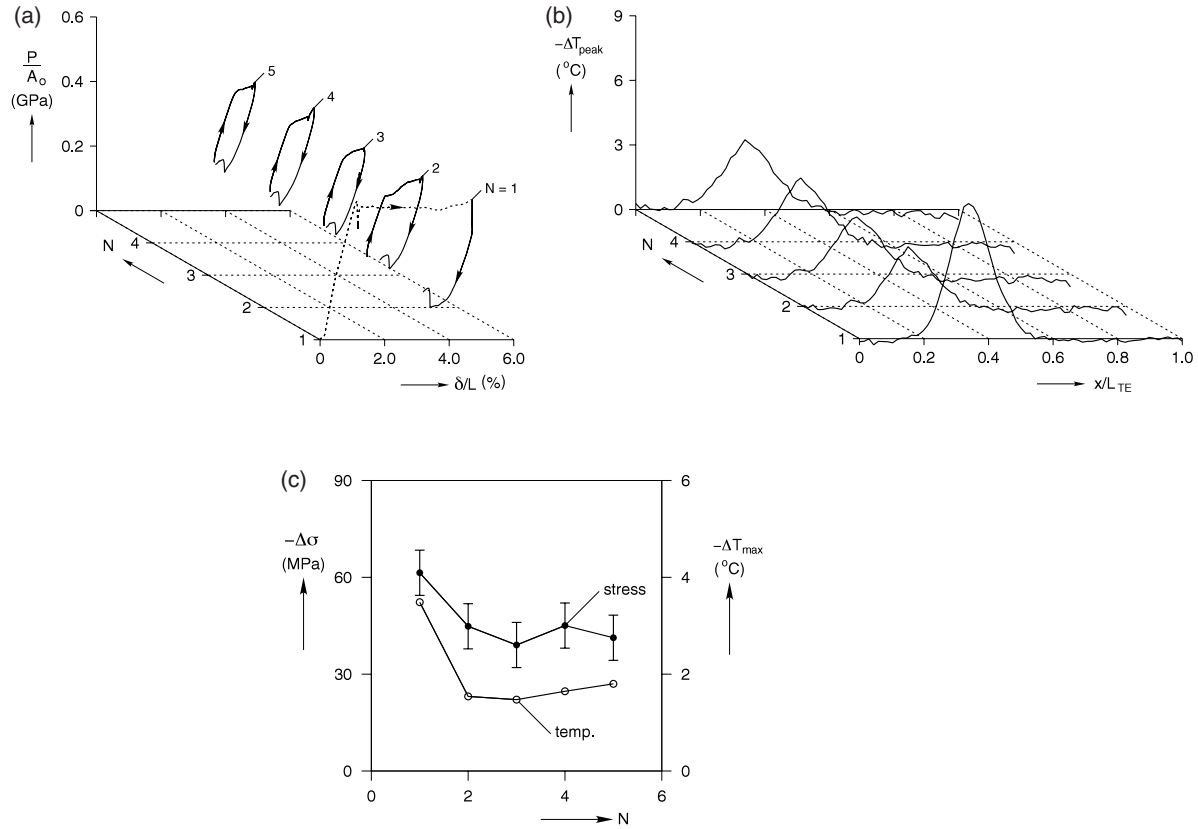

Figure 10. Results of experiment 3A performed at 14 °C: (a) load–displacement for the first five cycles; (b) change of temperature profiles at the time of peak temperature for the first five cycles; and (c) change in maximum stress and maximum temperature rise versus cycle number (uncertainties associated with the ΔT_{max} data points are less than the size of the data points shown).

the temperature of the remainder of the wire (see diagram in figure 4(c), $A \rightarrow M^+$ initiation), forcing first initiation at one of the cold 12 mm thermoelectric modules (figure 5(c), $A \rightarrow M^+$ initiation). After first initiation, the loading is paused and the 12 mm thermoelectric modules are heated to the same temperature as the two 6 mm thermoelectric modules (see $A \rightarrow M^+$ plateau in figure 4(c)). Loading is then continued until the entire length of the cooler region of the specimen (48 mm length in contact with all five thermoelectric modules, see figure 4(c) $A \rightarrow M^+$ plateau) has been transformed to martensite (figure 5(c), end loading segment). Figure 10(a) shows the mechanical response versus cycle number for a virgin specimen (experiment 3A). After initiation of localization $A \rightarrow M^+$ (see load drop in dotted line at end of initial elastic loading), the loading is paused and all thermoelectric modules are cooled to the same temperature ($T_{exp} = 14\,°C$). Loading is continued along a plateau stress, but the stress rises somewhat as fronts meet the hotter region outside the thermoelectric modules (figure 4(c), $A \rightarrow M^+$ plateau). After the entire cooled region (48 mm length) is transformed, $A \rightarrow M^+$ loading is stopped (end of dotted line). Two fronts now exist at the limits of this region (figure 5(c), end loading segment). All the thermoelectric modules are cooled, with the exception of one of the 6 mm thermoelectric modules (14 °C, experiment 3A) that defines the ROI (see figure 4(c), $M^+ \rightarrow A$ initiation). During this time the load drops, as shown in figure 10(a), with no change in displacement. The cold thermoelectric modules temporarily arrest the motion of the existing fronts located at the limits of the thermoelectric modules.

The specimen is then unloaded. Reverse transformation occurs through the motion of the existing fronts or a new initiation. $M^+ \rightarrow A$ transformation occurs once the stress reaches a low enough level (contrary to the $A \rightarrow M^+$ behavior). Recall, the transformation stress is a strongly increasing function of temperature. All of the thermoelectric modules (including the two 12 mm thermoelectric modules with existing fronts) are made cold enough compared to the 6 mm thermoelectric module (ROI), such that the $M^+ \rightarrow A$ initiation stress threshold in the ROI is above the $M^+ \rightarrow A$ propagation stress for the existing fronts (figure 5(c), $M^+ \rightarrow A$ initiation). This also prevents new initiation in the other 6 mm and middle 12 mm thermoelectric modules, and results in $M^+ \rightarrow A$ initiation occurring in the portion of the specimen in contact with the slightly warmer ROI ($T_{exp} = 14\,°C$, experiment 3A). At the $M^+ \rightarrow A$ initiation event there is a distinct stress rise in figure 10(a), and self-cooling due to endothermic transformation is seen in the temperature change profiles in figure 10(b) (note the negative temperature axis). After initiation, the loading is stopped, thus completing the first cycle. Subsequent cycles are performed with the same ambient temperature field (see figure 4(c), $M^+ \rightarrow A$ initiation). On loading, the existing austenite in the ROI transforms to martensite as the existing fronts propagate toward one another

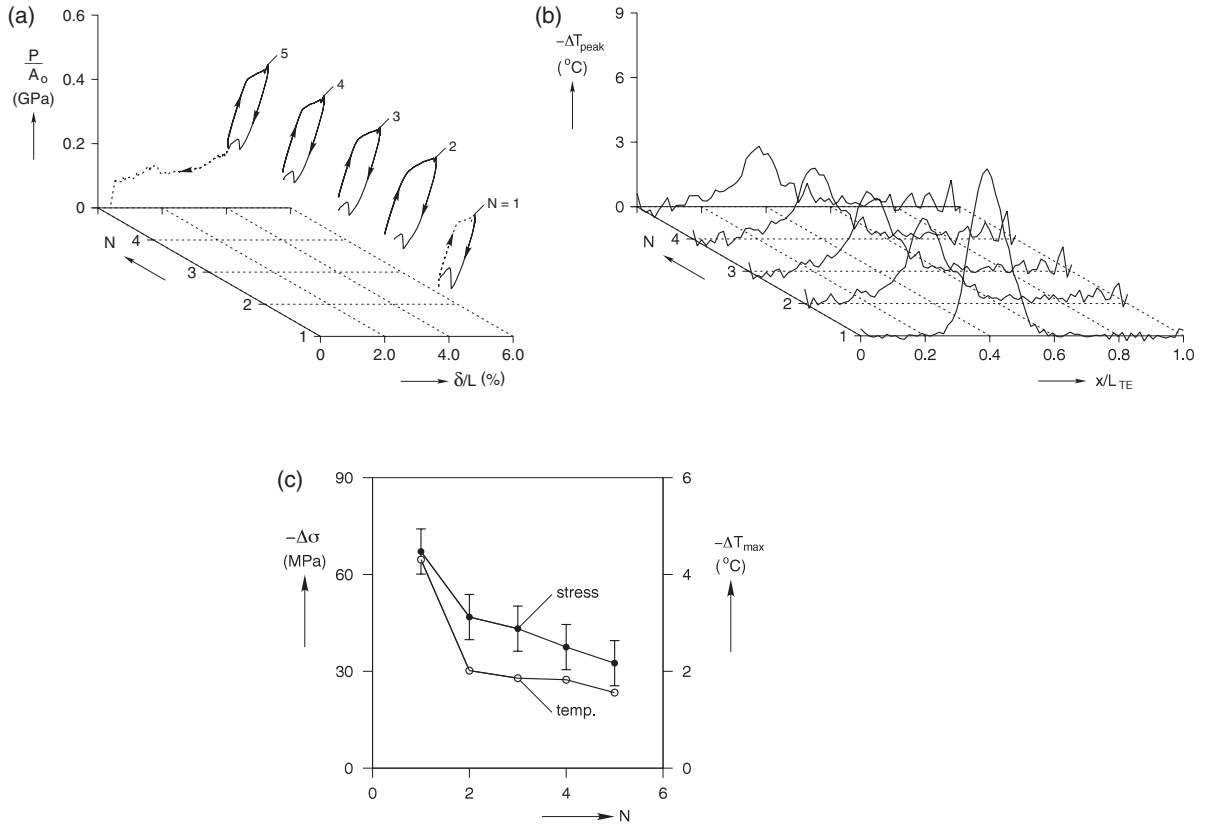

Figure 11. Results of experiment 3B performed at 26 °C: (a) load–displacement for the first five cycles; (b) change of temperature profiles at the time of peak temperature for the first five cycles; and (c) change in maximum stress and maximum temperature rise versus cycle number (uncertainties associated with the ΔT_{max} data points are less than the size of the data points shown).

and coalesce (see the small drop in load at the end of loading in cycle 2 and similar behavior in all subsequent cycles shown in figure 10(a)).

At the end of the loading plateau, the specimen is immediately unloaded. Again $M^+ \rightarrow A$ initiation is forced to occur in the region of interest, the initiation valley and temperature drop are clear in figures 10(a) and (b) for the first five cycles shown. Although the size of the peaks changes with cycle number in figure 10(b), the location for each peak along the length of the thermoelectric module is constant. This is similar to the behavior seen in experiment set 2, but now for $M^+ \rightarrow A$ initiation. The magnitudes of these peaks are plotted versus cycle number in figure 10(c) for all five cycles performed. Again we see a correlation between the latent cooling peaks and the stress rise at the initiation for each cycle.

The initiation of $M^+ \rightarrow A$ up to this point has been confined to the limits of the ROI (the chosen 6 mm thermoelectric module). A second series of $M^+ \rightarrow A$ initiation cycles is immediately performed at a higher temperature in a similar manner using a second 6 mm thermoelectric module as the ROI. Figure 11(a) shows the mechanical response for continued testing at the second ROI at a temperature of 26 °C, experiment 3B. Since this portion of the specimen has not undergone reverse transformation ($M^+ \rightarrow A$), it may be considered effectively a virgin ROI. With the former ROI still at the same temperature, the specimen is loaded until coalescence of the existing fronts ($M^+ \rightarrow A$), see dashed curve in figure 11(a) at the start of cycle 1 ($N = 1$). At the end of this loading, the 48 mm length in the center of the exposed length is now martensite (figure 5(c), after $A \rightarrow M^+$ coalescence). Then the new ROI (6 mm thermoelectric module) is heated to 26 °C to be the hottest region in the 48 mm martensite length. During unloading, $M^+ \rightarrow A$ initiation occurs within the ROI and a clear initiation stress rise is observed (figure 11(a)). Simultaneously, the change in temperature profile is observed (see figure 11(b)). This completes the first cycle in this ROI. The current ambient temperature field is maintained for the remaining four cycles shown in figure 11. A constant axial location and extent of the change in temperature valleys are seen in figure 11(b). The resulting valleys are plotted versus cycle number in figure 11(c), where we again see excellent correlation. After the last cycle, the specimen is fully unloaded (dotted line in figure 11(a) cycle 5) through the remaining portion of the transformation plateau to a final elastic unload. Similar to the observation in experiment set 2, the magnitudes of stress peaks/valleys and temperature peaks/valleys start larger at higher temperatures, but decay much more rapidly with cycling than at lower temperatures.

5. Conclusions

A thermo-mechanical experimental arrangement for testing various aspects of the onset of unstable mechanical behavior in pseudoelastic SMA wire is presented. Previous work has

shown that the rate dependence of SMA wire and the kinetics of transformation fronts are related to the size of the stress peaks at the onset of instability. The experimental setup presented here overcomes some of the difficulties in testing unstable thermo-mechanical behavior. It minimizes the effects of stress concentrations and restricts first initiation to a small portion of the free length (for both the $A \rightarrow M^+$ and $M^+ \rightarrow A$ initiations), while allowing a large range of temperature investigation and imaging during cyclic loading.

Multiple types of investigations are possible with minimal reconfiguration of the general experimental arrangement. Three experimental sets are presented showing the capability of the arrangement to observe (1) the dynamic nature of the initiation event (including its extent), and the size of the initiation peak and the associated latent heating temperature spike during (2) loading $A \rightarrow M^+$ transformation and (3) unloading $M^+ \rightarrow A$ transformation through repeated transformation cycles.

The first set of experiments, focusing on the dynamic initiation of $A \rightarrow M^+$ transformation, successfully captures the extent of the initiation region optically and the associated load drop and temperature spike over the first two seconds of the initiation. Although the initial temperature bloom is detectable with 60 Hz infrared imaging, the active temperature control quickly forces the wire temperature back to the isothermal state. The set includes two experiments at 22 and 34 °C. The change in temperature and extent of the localization associated with the initiation increase in magnitude with an increase in temperature (and transformation stress).

The second set of experiments looking at the repeated initiation of the $A \rightarrow M^+$ transformation shows that the location of the initiation is generally constant through multiple cycles and that the magnitude of the initiation stress peak and temperature spike decrease with cycle number. Since these decreases have similar trends, the reduction in the stress peak appears to be associated with reduced transformation (residual martensite) and damage in that area. The ability for the arrangement to be used at different set temperatures is demonstrated, as well as a method to use multiple portions of the same specimen as virgin samples for testing. For a 17 °C increase in experimental temperature, the magnitude of the stress drop and temperature spike became larger, but they decay away much more rapidly with cycling than for experiments at the lower temperature.

The final set of experiments investigates the repeated initiation of the $M^+ \rightarrow A$ transformation. Although this set requires some complications in the temperature control, the ability of the arrangement to accomplish the experiments at two temperatures using only one specimen is demonstrated. Again the location of the repeated initiations remained constant. The initiation peak size and temperature drop are seen to decrease in magnitude with cycle number. This last point has never been reported before, but seems reasonable considering the behavior seen in the second experiment. A second experiment is presented at a 12 °C increase in experimental temperature. However, little change is seen in the magnitude of the stress peak and temperature drop change with cycling between this second experiment and the first in this set.

In summary, an experimental configuration is demonstrated that can be used to measure the initiation of transformation in a shape memory alloy exhibiting unstable mechanical behavior, such as virgin NiTi. This configuration restricts the initiation to a small portion of the free length, permitting full-field optical tracking, infrared imaging (temperature measurement), use of laser extensometry, and the monitoring of load and extension. The arrangement can be used to capture events that occur at static to near dynamic rates. The temperature control apparatus keeps the specimen region of interest nearly isothermal, and large changes in experimental set temperatures can be selected by using temperature controlled circulating fluids and thermoelectric devices. The experimental configuration is capable of producing high quality data for a wide range of experiments (investigating the $A \rightarrow M^+$ and $M^+ \rightarrow A$ transformation initiations) for use in calibration of numerical models.

Acknowledgments

The authors would like to recognize the financial support of the National Research Council (for M Iadicola) and National Science Foundation (NSF CAREER grant for J Shaw) with sincere thanks.

References

Brinson L C, Schmidt I and Lammering R 2004 Micro and macromechanical investigations of transformation behavior of a polycrystalline NiTi shape memory alloy using in situ optical microscopy *J. Mech. Phys. Solids* **52** 1549–71

Gong J M, Tobushi H, Takata K, Okumura K and Endo M 2002 Cyclic superelastic deformation of TiNi shape-memory alloy *Mater. Sci. Forum* **394/395** 245–8

Iadicola M A and Shaw J A 2002a The effect of uniaxial cyclic deformation on the evolution of phase transformation fronts in pseudoelastic NiTi wire *J. Intell. Mater. Syst. Struct.* **13** 143–56

Iadicola M A and Shaw J A 2002b An experimental setup for measuring unstable thermo-mechanical behavior of shape memory alloy wire *J. Intell. Mater. Syst. Struct.* **13** 157–66

Iadicola M A and Shaw J A 2004 Rate and thermal sensitivities of unstable transformation behavior in a shape memory alloy *Int. J. Plast.* **20** 577–605

Kudva J N, Sanders B, Pinkerton-Florance J and Garcia E 2001 Overview of the DARPA/AFRL/NASA smart wing phase 2 program *Smart Structures and Materials 2001: Industrial and Commercial Applications of Smart Structures Technologies* vol 4332, ed A M R McGowan (Bellingham, WA: The International Society for Optical Engineering) pp 383–9

Liu Y, Liu Y and Van Humbeeck J 1998 Lüders-like deformation associated with martensite reorientation in NiTi *Scr. Mater.* **39** 1047–55

Nguyen T D, Carpenter B F and Hall J 2001 Flexible tab assisted control concept—flexTAC *Smart Structures and Materials 2001: Industrial and Commercial Applications of Smart Structures Technologies* vol 4332, ed A M R McGowan (Bellingham, WA: The International Society for Optical Engineering) pp 364–9

Otsuka K and Wayman C M (ed) 1998 *Shape Memory Materials* (Cambridge: Cambridge University Press)

Rey N M, Tillman G, Miller R M, Wynosky T, Larkin M J, Flamm J D and Bangert L S 2001 Shape memory alloy actuation for a variable area fan nozzle *Smart Structures and Materials 2001: Industrial and Commercial Applications of Smart Structures Technologies* vol 4332, ed A M R McGowan (Bellingham, WA: The International Society for Optical Engineering) pp 371–82

Schwartz M (ed) 2002 *Encyclopedia of Smart Materials* (New York: Wiley)

Shaw J A and Kyriakides S 1995 Thermomechanical aspects of NiTi *J. Mech. Phys. Solids* **43** 1243–81

Shaw J A and Kyriakides S 1997 On the nucleation and propagation of phase transformation fronts in a NiTi alloy *Acta Mater.* **45** 673–700

Shaw J A, Chang B-C, Iadicola M A and Leroy Y 2003 Thermodynamics of a 1-d shape memory alloy: Modeling, experiments, and applications *Smart Structures and Materials 2003: Modelling, Signal Processing, and Control* vol 5049, ed R C Smith (Bellingham, WA: The International Society for Optical Engineering) pp 76–87

Shaw J A 1997 Material instabilities in a nickel-titanium shape memory alloy *PhD Dissertation* The University of Texas at Austin, Department of Aerospace Engineering

Shaw J A 2000 Thermo-mechanical simulations of localized thermo-mechanical behavior in a NiTi shape memory alloy *Int. J. Plast.* **46** 541–62

Tse K K and Sun Q P 2000 Some deformation features of polycrystalline superelastic NiTi shape memory alloy thin strips and wires under tension *Key Eng. Mater.* **177–180** 455–60